Journal of Catalysis 260 (2008) 358–370

Contents lists available at ScienceDirect

Journal of Catalysis

www.elsevier.com/locate/jcat

Characterization of CeO_2-supported Cu–Pd bimetallic catalyst for the oxygen-assisted water–gas shift reaction

Elise B. Fox [a,1], Subramani Velu [a,2], Mark H. Engelhard [b], Ya-Huei Chin [b], Jeffrey T. Miller [c], Jeremy Kropf [d], Chunshan Song [a,*]

[a] Clean Fuels and Catalysis Program, EMS Energy Institute, and Department of Energy and Mineral Engineering, The Pennsylvania State University, 209 Academic Projects Building, University Park, PA 16802, USA
[b] Environmental and Molecular Science Laboratory, Pacific Northwest National Laboratory, Richland, WA 99352, USA
[c] BP Research Center, 150 W. Warrenville Road, Naperville, IL 60563-8406, USA
[d] Argonne National Laboratory, Argonne, IL 60430-4837, USA

ARTICLE INFO

Article history:
Received 22 June 2008
Revised 24 August 2008
Accepted 27 August 2008
Available online 23 October 2008

Keywords:
Catalyst
Bimetallic catalyst
Water–gas shift
Oxygen-assisted water–gas shift
CeO_2
Cu–Pd
Characterization
TPR
XPS
EXAFS

ABSTRACT

Our recent work demonstrated that Cu–Pd bimetallic catalyst supported on a nano-crystalline CeO_2 synthesized by urea gelation method is effective for oxygen-assisted water–gas shift (OWGS) reaction. The present study focuses on the roles of Cu and Pd in $CuPd/CeO_2$ bimetallic catalysts containing 20–30 wt% Cu and 0.5–1 wt% Pd used in the OWGS reaction employing a combined bulk and surface characterization techniques such as EXAFS, XRD, TPR, CO chemisorption, and *in situ* XPS. The catalytic activity for CO conversion and the stability of catalyst during on-stream operation increased by the addition of Cu to Pd/CeO_2 or Pd to Cu/CeO_2 monometallic catalysts, especially when the OWGS reaction was performed at low temperatures, below 200 °C. The TPR of monometallic Cu/CeO_2 showed reduction of CuO supported on CeO_2 in two distinct regions, around 150 and 250 °C. The high temperature peak disappeared and reduction occurred in a single step around 150 °C upon Pd addition. *In situ* XPS studies showed a shift in Cu 2p peaks toward lower binding energy (BE) with concomitant shift in the Pd 3d peaks toward higher BE. An inward diffusion of Pd into the CeO_2 support occurred upon reduction. On the other hand, inward diffusion of Cu occurred when Pd was present in the sample. These observations indicated the existence of synergistic interactions between Cu and Pd in these catalysts which could be responsible for the improved catalytic activity and stability of $CuPd/CeO_2$ bimetallic catalyst. The EXAFS analysis of Cu showed no clear evidence of Cu–Pd alloy formation at the copper edge. However, evidence for Pd–Cu alloy was shown in the Pd edge, and Pd atoms are surrounded only by Cu atoms in the reduced $CuPd/CeO_2$ bimetallic catalyst as revealed by EXAFS.

1. Introduction

Hydrogen (H_2) is considered to be a major clean energy carrier in the future because it can be used in more energy-efficient fuel cells and may be produced from various renewable and non-renewable sources [1–8]. Catalytic reforming of gaseous and liquid hydrocarbons, carbohydrates and alcohol fuels is an attractive option for hydrogen (H_2) generation for proton-exchange membrane (PEM) fuel cells. One of the down falls in generating H_2 by reforming these fuels is the co-production of large amounts of CO, which is a poison to fuel cell anode catalysts when the CO concentration in the reformed gas exceeds 30 ppm. The CO is therefore removed in the downstream by water–gas shift (WGS) reaction or a combined WGS and preferential oxidation (PrOx) reactions. Consequently, the downstream CO clean up step occupies over 50% of the volume of the reforming process, making it highly inconvenient, especially for onboard production of H_2 for fuel cell applications [9]. Furthermore, the catalysts used are mainly Cu-based, which is pyrophoric and undergo rapid deactivation during on-stream and repetitive start-up-and-stop operations [10,11]. Improved WGS process and catalysts are therefore required in order to reduce the catalyst volume and hence the size of the reactor [12].

We have recently reported on the oxygen-assisted water–gas shift (OWGS) reaction over CeO_2 supported Cu–Pd bimetallic catalysts [13], wherein a small amount of oxygen is added in the WGS reactions, as an efficient process for removing CO from the reformed gas at relatively lower temperature. It is believed that the added oxygen promotes the WGS reaction by facilitating the adsorption and decomposition of water [14,15]. A systematic study has been performed to optimize the CeO_2 preparation method,

* Corresponding author. Fax: +1 814 865 3573.
E-mail address: csong@psu.edu (C. Song).
[1] Present address: Savannah River National Laboratory, 999-2W, Aiken, SC 29808.
[2] Present address: Refining Technology, BP Products North America, Inc., 150 West Warrenville Road, Naperville, IL 60563, USA.

0021-9517/$ – see front matter
doi:10.1016/j.jcat.2008.08.018

metal loadings and the method of metal loadings, reaction operating conditions and so on in order to achieve high CO conversion efficiency. A high catalytic performance has been observed over Cu–Pd bimetallic catalysts with a Cu loading between 20 and 30 wt% and Pd loading between 0.5 and 1 wt% supported on nano-crystalline CeO_2 synthesized by urea gelation method. Better catalytic performance has been observed over Cu–Pd bimetallic catalyst than monometallic catalyst containing either Cu alone or Pd alone supported on the CeO_2 support. However, the role of Cu and Pd on the catalytic performance in the OWGS reaction and the surface nature of the Cu–Pd bimetallic catalysts have not been well understood.

The objective of the present work was therefore to investigate the roles of Cu and Pd in the $CuPd/CeO_2$ bimetallic catalyst for the OWGS reaction through detailed characterization. The catalysts have been characterized by various analytical and spectroscopic techniques, including pseudo *in situ* X-ray photoelectron spectroscopy (XPS) and extended X-ray absorption, fine structure (EXAFS) spectroscopy to understand the nature of the catalysts and to correlate the properties with the catalytic performance.

2. Experimental

2.1. Catalysts preparation and characterization

The support CeO_2 was prepared by urea gelation method as described elsewhere and had a BET surface area of about 215 m^2/g [13]. Cu and Pd metals were deposited onto the support surface by incipient wetness impregnation (IWI) method, where a minimum amount of solvent is used to deposit the metal on the substrate. The support saturation limit was determined by adding solvent drop by drop. The limit (the incipient wetness volume) was determined to be 0.5 mL/g for CeO_2 prepared by urea gelation. Cu salt [$Cu(NO_3)_2{\cdot}2.5H_2O$] was first dissolved in deionized water then added drop by drop to the support. After all of the solution was added, a small amount of water was used to rinse the beaker and add residual salt. The mixture was then placed in an oven at 120 °C. Due to high copper loads this step was repeated until all the desired Cu salt was added. The Pd salt [$Pd(CH_3COO)_2$] was then dissolved in acetone and added drop by drop. The bimetallic catalyst was oven dried at 120 °C for 1 h. After drying the catalysts were calcined to 400 °C at a heating rate of 2 °C/min and held for 3–4 h. The monometallic catalysts were prepared in the same manner using the appropriate salt solution. All catalysts were reduced under 5% H_2 in Ar at a heating rate of 5 °C/min up to 225 °C and held for 1 h.

Experimental details concerning the elemental analysis by ICP-AES, temperature programmed reduction (TPR), X-ray diffraction (XRD) and the BET surface area of the unreduced catalysts were determined as previously described [13,16]. The metal dispersions were determined by CO chemisorption method on a Micromeritics AutoChem 2910 TPR/TPD instrument that was used for the TPR experiments. A 10.5% CO–He gas mixture was used as a probe molecule. The sample was pre-reduced *in situ* at 5 °C/min to 225 °C, held for 30 min followed by cooling down to ambient temperature. The chemisorption data were collected step-wise at 50 °C. The total metal dispersion was calculated from the CO chemisorption data using the following equation

$$\mathrm{PD} = 100\left(\frac{V_s \mathrm{SF}}{\mathrm{SW} \times 22{,}414}\right)\mathrm{GMW}_{\mathrm{calc}}, \tag{1}$$

where V_s is the volume of absorbed gas, SF is the calculated stoichiometric factor, which is taken as 1 for both Pd and Cu, SW is the sample weight, and GMW is the calculated gram molecular weight in g/mol.

X-ray absorption measurements were made on the insertion-device beam line of the Materials Research Collaborative Access Team (MRCAT) at the Advanced Photon Source, Argonne National Laboratory. A cryogenically cooled double-crystal Si (111) monochromator was used in conjunction with an uncoated glass mirror to minimize the presence of harmonics. The monochromator was scanned continuously during the measurements with data points integrated over 0.5 eV for 0.07 s per data point. Measurements were made in transmission mode with the ionization chambers optimized for the maximum current with linear response ($\sim 10^{10}$ photons detected/s) using a mixture of nitrogen and helium in the incident X-ray detector and a mixture of ca. 20% argon in nitrogen in the transmission X-ray detector. A copper foil, or Pd foil, spectrum was acquired simultaneously with each measurement for energy calibration.

Dried catalyst samples were pressed into a cylindrical holder with a thickness chosen to give a total absorbance (μx) at the Cu*K* (8.979 keV) edge, or Pd*K* (24.350 keV) edge, of about 2.0 and an edge step ($\Delta\mu x$) of ca. 0.5. The catalysts were treated in a continuous-flow EXAFS reactor cell (18 in. long, 0.75 in diam.) fitted at both ends with polyimid windows and valves to isolate the reactor from the atmosphere. The spectra were obtained at room temperature. The Cu catalysts were analyzed as received and reduced at 250 °C for 30 min in of 4% H_2/He. The Pd catalysts were analyzed after reduction in 4% H_2/He at 300 °C for 30 min followed by purging with He at 300 °C for 30 min to desorb chemisorbed hydrogen and decompose Pd-H.

Phase shifts, backscattering amplitudes and XANES references were obtained from reference compounds: CuO (Aldrich), $Cu(H_2O)_6{\cdot}2.5H_2O$ (Aldrich), Cu_2O (Aldrich), Cu foil and Pd foil. Theoretical phase and amplitude functions were calculated for Pd–Cu backscattering pair using FEFF8. The Cu XANES fits from 8.95 to 9.02 keV of the normalized spectra were made by linear combination of experimental standards. Standard procedures based on WINXAS97 software were used to extract the EXAFS data. The coordination parameters were obtained by a least square fit in *q*- and *r*-space of the isolated nearest neighbor, k^2-weighted Fourier transform data. The data fit equally well with both k^1 and k^3 weightings.

XPS measurements of both unreduced as well as reduced catalysts were performed by a "pseudo *in situ* method" at the Environmental Molecular Sciences Laboratory facility, Pacific Northwest National laboratory [17]. About 100 mg of the catalysts were loaded in a quartz reactor and reduced under 5% H_2/Ar mixture (50 cc/min). The samples were reduced at a heating rate of 5 °C/min up to 225 °C and kept at this temperature for 1 h before cooling down to room temperature. The reactor was sealed and transferred into a glove box with O_2 concentration maintained below 0.4 ppm. In the glove box, the reduced catalysts were retrieved and mounted for XPS analysis. The samples were then loaded into the XPS chamber without exposing to air. The XPS data were acquired on a Physical Electronics Quantum 2000 Scanning ESCA Microprobe instrument using a focused monochromatic Al$K\alpha$ X-ray source (1486.7 eV). The vacuum at the spectrometer and the sample introduction chamber were 1.8×10^{-9} and 1.5×10^{-6} Torr, respectively. The BE scale was calibrated using the BEs of Au $4f_{7/2}$, Ag $3d_{5/2}$, and Cu $2p_{3/2}$ at 83.96, 368.21, and 932.62 eV, respectively. The data were collected using a pass energy of 46.95 eV and referenced using the BE of Ce $3d_{3/2}$ $4f^0$ at 917 eV. The surface chemical compositions are quantitatively determined from the high energy resolution data using peak areas after Shirley background subtraction and atomic sensitivity factor of elements: O (0.733), Cu (2.626), Pd (5.637), Ce (12.0), and C (0.314). The surface carbon was detected in all samples, but not included in the calculation of surface composition.

Table 1
Physicochemical properties of unreduced CeO_2 supported CuPd-bimetallic catalysts.

Catalyst	[a]SA_{BET} (m^2/g)	[b]Metal dis. (%)	[c]Metal loadings (wt%)		[d]Crystallite size (nm)		[e]*d*-Interplanar spacing (nm)	
			Cu	Pd	CuO	CeO_2	CuO	CeO_2
Pd/CeO_2	156	38.5	–	0.5	–	3.86	–	0.20
Cu/CeO_2	62	0.5	18.1	–	7.54	6.46	0.17	0.20
$CuPd/CeO_2$	97	0.8	25.0	0.5	9.42	6.94	0.17	0.20
$CuPd/CeO_2$–NH_3 leach	62	1.0	20.5	0.6	10.32	7.88	0.18	0.20
$CuPd/CeO_2$–HNO_3 leach	93	29.3	0.9	0.3	ND	5.70	ND	0.20
$CuPd(1)/Al_2O_3$	7	0.3	20.4	0.4	ND	–	ND	–
$Cu/ZnO–Al_2O_3$[f]	[f]60	–	[f]42.0	–	ND	–	ND	–

ND = not determined.
[a] BET surface area determined by N_2 adsorption.
[b] Metal dispersions determined by CO chemisorption measurements.
[c] Determined by ICP-AES.
[d] Determined by Debye–Scherrer equation at the Cu(111) and CeO_2(111) peaks.
[e] Determined by the Bragg equation at the (111) peak, 0.31248 nm for CeO_2 (ICDD #81-0792) and 0.25444 nm for CuO (ICDD #44-0706).
[f] As reported by the manufacturer, Süd Chemie for the commercial $Cu/ZnO–Al_2O_3$ catalyst: C18-7-01.

2.2. Catalytic studies

Oxygen-assisted water–gas shift (OWGS) reaction was performed in the temperature range between 180 and 240 °C in a fixed-bed down-flow reactor as described earlier [13]. A dry gas mixture containing 4% CO, 10% CO_2, 2% compressed air, 26% Ar and balance (about 60%) H_2 was used as received. This gas mixture was then combined with steam at a CO/H_2O molar ratio of 1/10. Steam was generated by passing distilled water at a fixed flow rate using a HPLC pump through a heated line kept around 140 °C. The effluent of the reactor was analyzed on-line using an Agilent 3000 A Micro GC equipped with thermal conductivity detectors with a CO detection limit of below 10 ppm. Prior to the reaction, the catalyst was reduced *in situ* at 225 °C for 1 h in H_2 flow. Commercial catalyst was reduced at 300 °C as was determined to be optimal temperature under previous experiments. All catalytic studies were repeated at least once to insure reproducibility of the results.

3. Results

3.1. Catalytic activity

The CeO_2 supported Cu–Pd bimetallic catalysts tested in the present study, their chemical compositions and textural properties are summarized in Table 1. The fresh catalysts contained Cu loadings between 20 and 25 wt% and Pd loading around 0.5 wt%. These catalysts have been tested in the OWGS reaction in the temperature range between 180 and 240 °C continuously for a period of about 72 h (3 days).

Fig. 1 displays the effect of temperature on the OWGS reaction over monometallic Pd/CeO_2 and Cu/CeO_2 catalysts and a bimetallic $CuPd/CeO_2$ catalyst compared at 35 h on-stream (top panel) and 70 h on-stream (bottom panel). A comparison of data at 35 h on-stream operation (top panel) indicates that, at 180 °C, the monometallic Pd/CeO_2 and Cu/CeO_2 catalysts exhibit about 60% CO conversion. The bimetallic $Cu–Pd/CeO_2$ catalyst shows a higher conversion of about 70%. The CO conversion increases with increasing reaction temperature and attains about 100% at 240 °C on all the catalysts. The data compared at 70 h on-stream operation (bottom panel) also show similar trend. However, due to catalysts deactivation, the CO conversion dropped to about 40% over the monometallic Pd/CeO_2 while the conversion remains almost unchanged over Cu/CeO_2 and $CuPd/CeO_2$ catalysts. It can also be noticed that, although the monometallic Pd/CeO_2 exhibits the lowest CO conversion, especially at 70 h on-stream operation at 180 °C, the catalyst exhibits the highest conversion of about 85% at 210 °C.

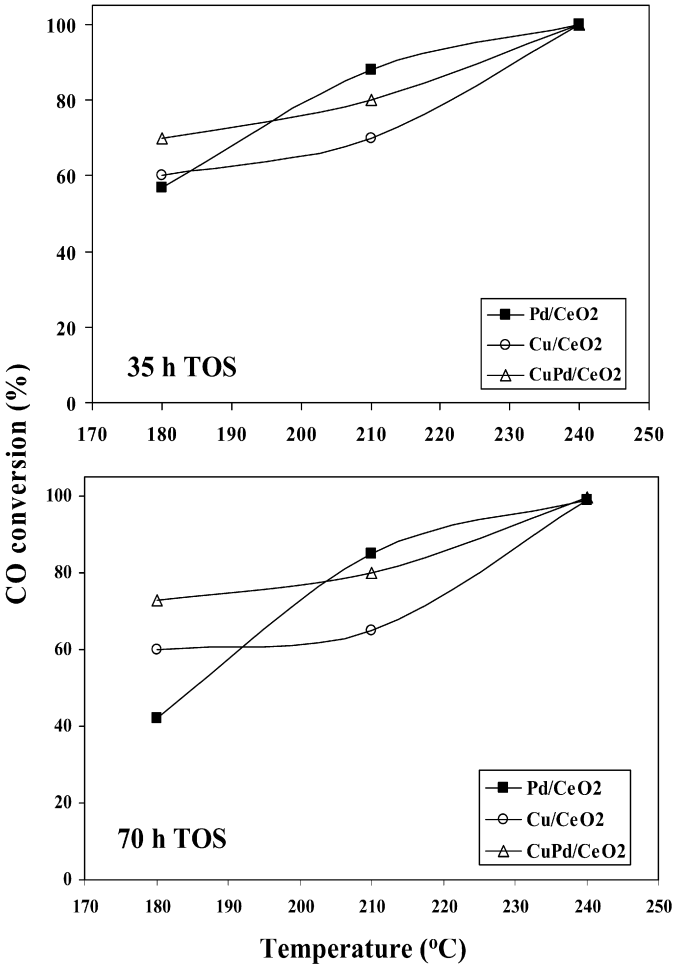

Fig. 1. Effect of Pd loading on CO conversion at different temperatures over CeO_2 supported CuPd-bimetallic catalysts in the OWGS reaction under H_2-rich atmosphere. (Top panel) Data collected around 35 h time-on-stream; (bottom panel) data collected around 70 h time-on-stream. Experimental conditions: temp. = 180–240 °C; CO/air = 1/0.5; CO/H_2O = 1/10; CO: 4%; CO_2: 10%; 26% Ar and balance H_2. GHSV = 24,000 h^{-1}.

Fig. 2 shows the time-on-stream (TOS) performance of the monometallic and bimetallic catalysts collected at 180 °C continuously for a period of 72 h (3 days). For comparison, the performance of a Cu–Pd bimetallic catalyst supported on Al_2O_3 ($Cu–Pd/Al_2O_3$) has also been included in the figure. The data collected are somewhat scattered, within ±10% CO conversion levels. It is

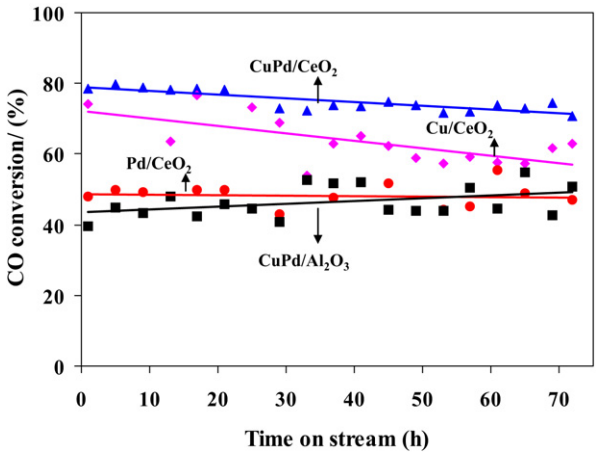

Fig. 2. Effect of Pd on the stability of CeO_2 supported CuPd-bimetallic catalysts in the OWGS reaction under H_2-rich atmosphere. Experimental conditions: temp. = 180 °C; CO/air = 1/0.5; CO/H_2O = 1/10; CO: 4%; CO_2: 10%; 26% Ar and balance H_2. GHSV = 24,000 h^{-1}.

probably due to the sequential catalyst deactivation-self regeneration of catalyst under the present operating conditions, experimental error or both. However, for better understanding of the performance of the catalyst during on-stream operation, straight lines have been drawn passing the line between the points. The results then indicate that the monometallic Pd/CeO_2 shows the lowest CO conversion of about 50% as an average with a slight deactivation. On the other hand, the monometallic Cu/CeO_2 exhibits an initial CO conversion of about 75%, but undergoes deactivation to about 60% CO conversion within 70 h. However, the $CuPd/CeO_2$ bimetallic catalyst exhibits much higher initial CO conversion, close to 80% and the conversion remains almost unchanged. The results thus imply that an improved catalytic activity and stability could be achieved when both Pd and Cu are present together.

The monometallic Pd/CeO_2 and Cu/CeO_2 catalysts are well known for the WGS and CO oxidation reactions [18–23]. These catalysts are known to undergo deactivation during on-stream operations. Wang et al. [19] have studied the deactivation mechanisms for Pd/CeO_2 during the WGS reaction through accelerating aging tests at 250 and 400 °C. It has been found that the deactivation is due to loss of Pd surface area.

The beneficial effect of CeO_2 support compared to the Al_2O_3 in the catalytic performance of Cu–Pd bimetallic catalysts in the OWGS reaction can be clearly seen from the data. The Al_2O_3 supported catalyst exhibits the lowest CO conversion of about 40%. The CO conversion is doubled when the Al_2O_3 support is replaced by CeO_2, which suggests that the redox properties and probably the strong metal–support interactions of CeO_2 support also play an important role in the reaction. In fact, CeO_2 is known to participate in the WGS as well as in CO oxidation catalysis [19,22,24]. The reaction has been reported to occur through a bifunctional redox mechanism in which CO adsorbed on the supported metal (Pd or Cu) is oxidized by CeO_2, which in turn, is oxidized by water.

The scanning electron microscopy (SEM) of the $CuPd/CeO_2$ catalyst used in the present study indicated the existence of separate Cu-rich and CeO_2-rich regions [13]. This raised a question if the bulk CuO or small CuO clusters dispersed on CeO_2 are active in the OWGS reaction. In order to investigate this phenomenon, leaching studies have been undertaken over these catalysts. The $Cu–Pd/CeO_2$ bimetallic catalyst has been treated separately in HNO_3 or in 30% aqueous NH_3 solution (NH_4OH) and leached for 15 h. As can be seen from the data in Table 1, only about 5 wt% loss in Cu content has been observed by NH_3 leaching, while HNO_3 leaching removed most of the CuO and also about 50% of PdO. OWGS reaction has been performed over these leached samples under the same experimental conditions used for the $CuPd/CeO_2$ bimetallic catalyst and the results after 35 h of on-stream operation are compared in Fig. 3. Since the performance of the leached samples was very poor at 180 °C, the data collected at 240 °C are compared. The catalytic performance of a commercial $Cu/ZnO–Al_2O_3$ catalyst containing about 40% Cu has also been compared under the same experimental conditions.

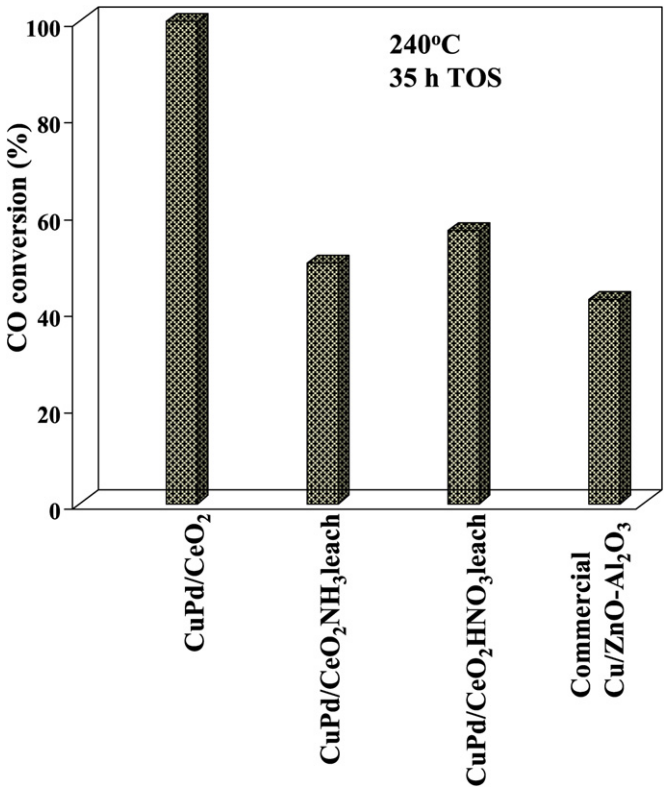

Fig. 3. Effect of leaching on the catalytic activity of CeO_2 supported CuPd-bimetallic catalysts in the OWGS reaction under H_2-rich atmosphere. Experimental conditions: temp. = 180 °C; CO/air = 1/0.5; CO/H_2O = 1/10; CO: 4%; CO_2: 10%; 26% Ar and balance H_2. GHSV = 24,000 h^{-1}.

As can be seen from the figure, the commercial $Cu/ZnO–Al_2O_3$ catalyst exhibits the lowest CO conversion of about 40%, compared to the $CuPd/CeO_2$ fresh catalyst, which exhibits about 100% CO conversion under the same experimental conditions. On the other hand, the conversion dropped to about 50% over the NH_3 leached sample ($CuPd/CeO_2$ NH_3 leach) and to about 60% over HNO_3 leached sample ($CuPd/CeO_2$ HNO_3 leach). Note that the Cu and Pd contents in the $CuPd/CeO_2$ NH_3 leached sample are close to that of the fresh $CuPd/CeO_2$ bimetallic catalyst. The lower catalytic performance after NH_3 leaching could be due to poisoning of the catalyst surface by NH_3. On the other hand, the HNO_3 leached sample, although the Cu content has been reduced to about 1 wt% and the Pd to about 0.3%, the catalyst still exhibits about 60% CO conversion. The loss of about 50% Pd together with Cu could account for the observed decrease in CO conversion. It should be noted that the catalyst containing about 1 wt% Cu and 1 wt% Pd supported on CeO_2 exhibited lower conversion than a catalyst containing about 25 wt% Cu and 1 wt% Pd [13]. This implies that copper loading has an impact on the performance of the $CuPd/CeO_2$ catalysts in the OWGS reaction. The observed results are in contrast to Liu et al. [25] and Li et al. [21], who have observed no appreciable difference in catalytic activity with increasing Cu content of Cu supported on La modified CeO_2 catalysts in WGS and CO oxidation reactions. However, the nature of the catalyst and the reaction conditions used in the present study are completely different from those earlier studies. Consequently, the structural and

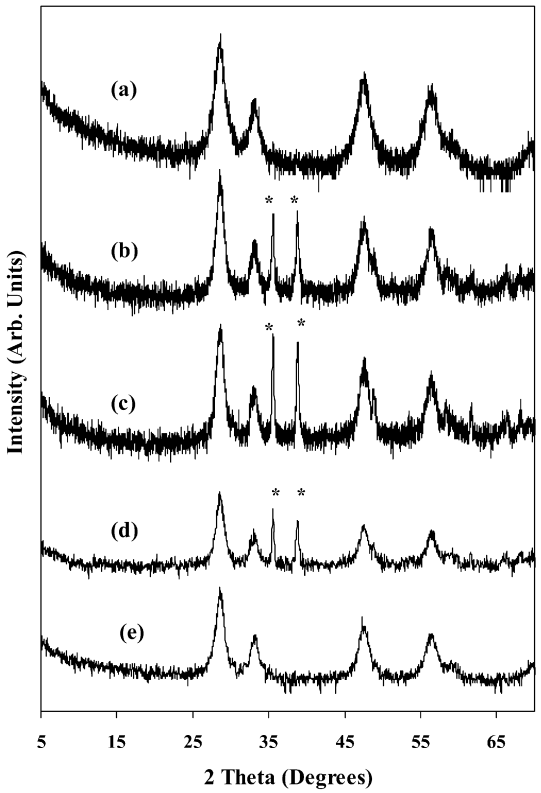

Fig. 4. XRD patterns of (a) Pd/CeO_2; (b) Cu/CeO_2; (c) $CuPd/CeO_2$; (d) $CuPd/CeO_2$–NH_3 leach; (e) $CuPd/CeO_2$–HNO_3 leach. ∗ indicates peaks corresponding to CuO.

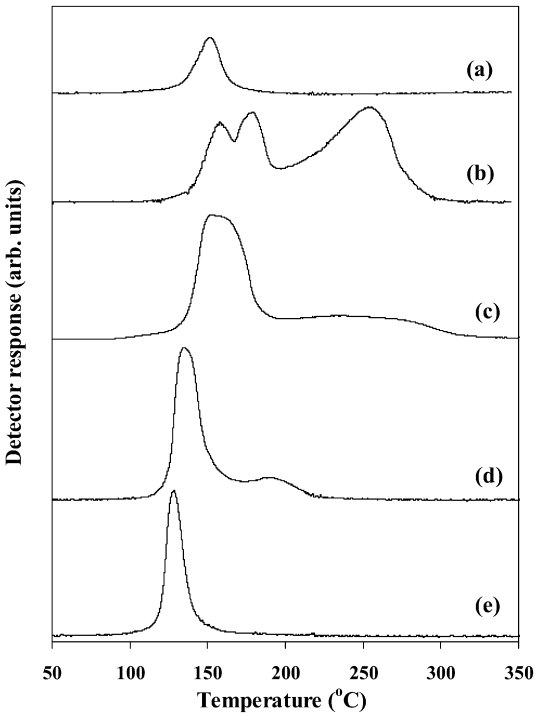

Fig. 5. TPR profiles of (a) Pd/CeO_2; (b) Cu/CeO_2; (c) $CuPd/CeO_2$; (d) $CuPd/CeO_2$–NH_3 leach; (e) $CuPd/CeO_2$–HNO_3 leach.

redox properties of the catalysts of the present study have been investigated by EXAFS, XRD, TPR and *in situ* XPS measurements in order to further understand the observed phenomenon and the results are discussed in the following sections.

3.2. Catalysts characterization

3.2.1. Bulk properties

The bulk properties of the catalysts are investigated by XRD and TPR experiments. Fig. 4 depicts the XRD patterns of CeO_2 supported Cu–Pd bimetallic catalysts while the crystallite sizes of CuO and CeO_2 determined by Scherrer equation are included in Table 1. As can be seen, all samples show characteristic CeO_2 peaks centering around 29, 33, 48 and 57° two theta and these peaks correspond to (111), (200), (220) and (311) planes, respectively. In addition to the CeO_2 peaks, sharp peaks centering around 36 and 39° two theta are also observed in the Cu-containing samples and they are attributed to (111) and (200) planes of CuO crystals. These peaks are relatively sharp and narrower compared to CeO_2 peaks and this is in line with earlier reports [21,25]. The crystallite sizes of CuO particles as calculated from Scherrer equation are in the range between 7 and 10 nm. Peaks corresponding to PdO are not observed probably due to the low weight percent of PdO (below 1 wt%) in the catalyst. This also suggests that small crystals (<5 nm) of the PdO particles, which are undetectable by XRD, are dispersed on the CeO_2 support.

The CeO_2 supported Cu–Pd bimetallic catalysts leached with NH_3 also exhibit peaks corresponding to CeO_2 and CuO while the sample leached with HNO_3 shows only the CeO_2 phase, suggesting that the finely dispersed CuO particles (<5 nm), are present in the HNO_3 leached samples. It should be recalled that, HNO_3 leaching decreases the Cu concentrations from about 25 to about 1 wt% and the Pd loading from 0.5 to 0.3 wt% (Table 1). The intensities of peaks for CeO_2 and CuO are dramatically decreased in the leached samples, implying that leaching processes also decrystallizes the sample.

The redox properties of the catalysts have been investigated by TPR experiments and the results are presented in Fig. 5. The monometallic Pd/CeO_2 catalyst without Cu shows a single reduction peak centering at 153 °C, and this can be attributed to the reduction of PdO interacting with the CeO_2 support. On the other hand, the Cu/CeO_2 catalyst exhibits reduction peaks at two different temperature regions, one below 200 °C, with a doublet centering at 159 and 179 °C, and the other above 200 °C. The peak below 175 °C has been generally assigned to the reduction of dispersed CuO clusters while the peak above 200 °C has been attributed to the reduction of CuO particles, similar to that of bulk CuO [24]. Interestingly, the $CuPd/CeO_2$ bimetallic catalyst possesses an intense peak centering around 160 °C together with a broad envelop up to 310 °C, indicating the formation of at least two different CuO clusters dispersed on the CeO_2 support together with some bulk-like CuO particles. No separate peak for the reduction of PdO could be seen, suggesting that the presence of Pd along with Cu makes the CuO and PdO reduction as a single broad peak. This reveals that in addition to the Pd–Ce and Cu–Ce interactions, a Cu–Pd interaction also exists in the present catalyst system. The synergistic interaction between Cu and Pd further improves the reducibility of Cu species.

The sharp peak centering at 130 °C in the HNO_3 treated sample can be attributed to the reduction of CuO clusters highly dispersed on the CeO_2 and interacting closely with PdO. The sharpening of the peak and the absence of the high temperature shoulder clearly indicates that significant amounts of bulk-like CuO species were removed by the HNO_3 treatment. Similar sharp peak at low temperature can also be observed together with an additional shoulder around 200 °C in the NH_3 treated sample, suggesting that the sample consists of significant amount of bulk-like CuO.

3.2.1.1. Cu EXAFS and XANES The XANES from 8.95 to 9.02 keV of CuO, Cu_2O and Cu foil references are given in Fig. 6 and the EXAFS in Fig. 7. Linear combination of these reference spectra were

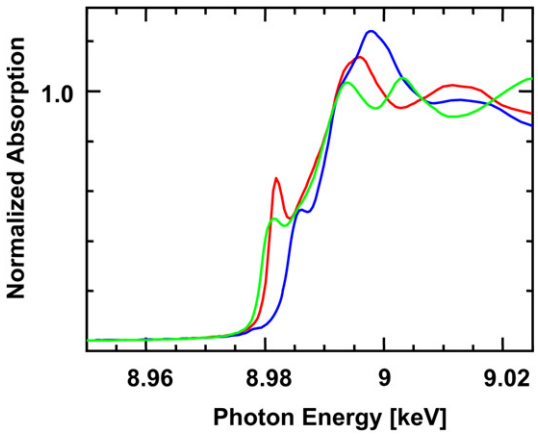

Fig. 6. XANES Cu reference compounds (8.95–9.02 eV). Red: Cu_2O; blue: CuO; green: Cu foil. (For interpretation of the references to color in this figure legend, the reader is referred to the web version of this article.)

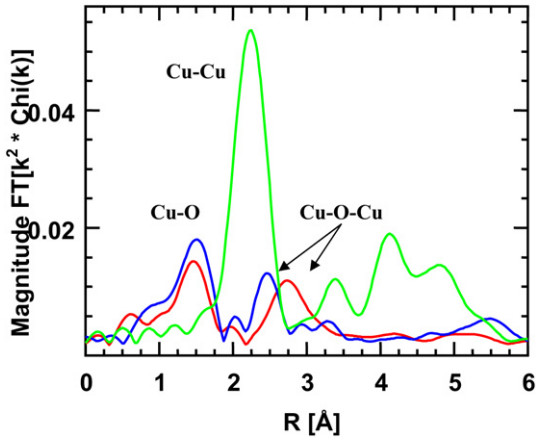

Fig. 7. EXAFS of Cu reference compounds (k^2: $\Delta k = 2.75$–12.2 Å^{-1}). Red: Cu_2O, $N_{Cu-O} = 2$, $R = 1.85$ Å; blue: CuO, $N_{Cu-O} = 4$, $R = 1.96$ Å; green: Cu foil, $N_{Cu-Cu} = 12$, $R = 2.55$ Å. (For interpretation of the references to color in this figure legend, the reader is referred to the web version of this article.)

Table 2
Cu XANES and EXAFS fits.

Sample	Treatment	XANES	Backscatter	CN	R	DWF	E_0
30% Cu–1% Pd/CeO_2	Air	1.0 CuO	Cu–O	3.9	1.94	0.0031	−9.8
	H_2 at 250 °C	1.0 Cu^0	Cu–Cu	10.1	2.55	0.0001	0.1
30% Cu/CeO_2	Air	1.0 CuO	Cu–O	4.0	1.94	0.0031	−9.5
	H_2 at 250 °C	1.0 Cu^0	Cu–Cu	8.9	2.55	0.0001	0.3
30% Cu–1% Pd/Al_2O_3	Air	1.0 CuO	Cu–O	4.2	1.94	0.0031	−9.0
	H_2 at 250 °C	1.0 Cu^0	Cu–Cu	10.0	2.55	0.0001	−0.6

fit to the catalyst samples. The XANES fits of all samples in air was consistent with CuO, Table 2. A typical fit is shown in Fig. 8 for 30% Cu/CeO_2. Coordination numbers and bond distances were determined from fitting the magnitude and imaginary parts of the Fourier transform. A typical fit for the first shell, i.e, Cu–O, of 30% Cu–1% Pd/Al_2O_3 in air is shown in Fig. 9. An N_{Cu-O} of 4.2 at a bond distance of 1.94 Å is also consistent with CuO. The higher shell Cu–O–Cu distance was not fit, but is at a position similar to the higher shell of CuO, which confirms TPR results.

The XANES fits of all samples treatment at 250 °C in 4% H_2/He indicated that the Cu was completely reduced. The EXAFS fits of the first shell are given in Table 2 and the magnitude of the Fourier transform of the catalysts and Cu foil is shown in Fig. 10. The bond distance of 2.55 Å for all catalysts is consistent with metallic Cu. The N_{Cu-Cu} of 30% Cu–1% Pd/CeO_2 and 30% Cu–1% Pd/Al_2O_3 is slightly larger than that of 30% Cu/CeO_2, 10 and 9, respectively. An estimate of the particle size from the N_{Cu-Cu} indicates that the metallic Cu particles in 30% Cu/CeO_2 is about 40 Å, while those in 30% Cu–1% Pd/CeO_2 and 30% Cu–1% Pd/Al_2O_3 are approximately

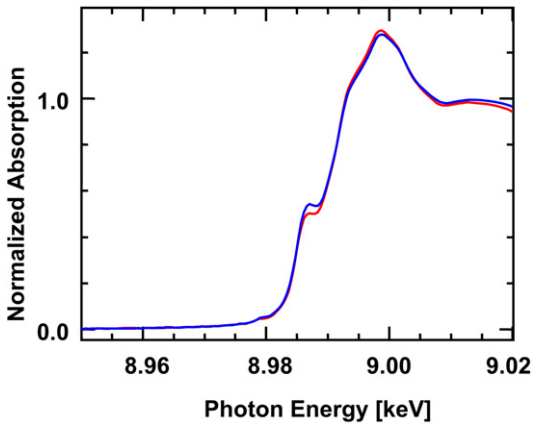

Fig. 8. XANES fit from 8.95 to 9.02 keV for Cu/CeO_2 in air. Red: data; blue: fit, 1.0 Cu_2O. (For interpretation of the references to color in this figure legend, the reader is referred to the web version of this article.)

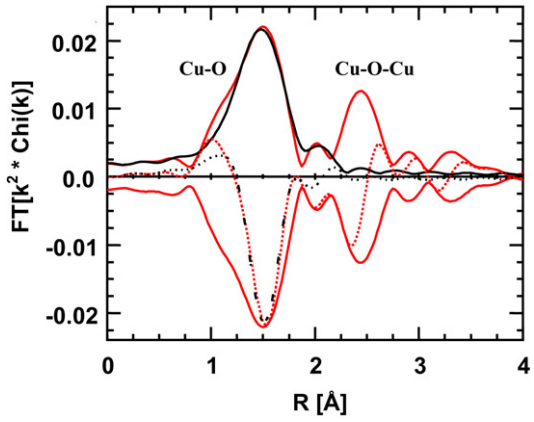

Fig. 9. Fit of first shell (Cu–O) of $CuPd/Al_2O_3$ in air (k^2: $\Delta k = 2.7$–12.0 Å^{-1}, $\Delta R = 0.9$–1.9 Å). Red solid: data-real part of FT; red dotted: data-imaginary part of FT; black solid: fit-real part of FT; black dotted: fit-imaginary part of FT; fit: $N_{Cu-O} = 4.2$, $R = 1.94$ Å. (For interpretation of the references to color in this figure legend, the reader is referred to the web version of this article.)

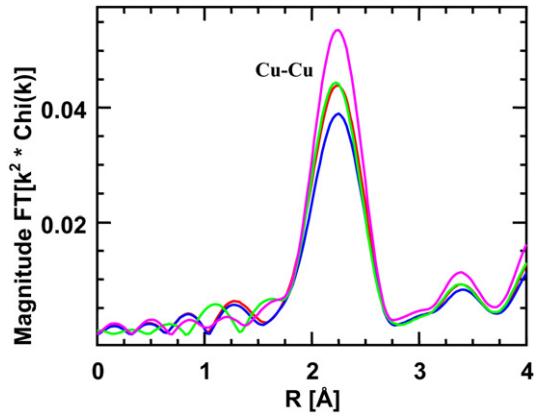

Fig. 10. Magnitude of FT for Cu catalysts reduced at 300 °C (k^2: $\Delta k = 2.7$–12.0 Å^{-1}, $\Delta R = 0.9$–1.9 Å). Red: $CuPd/CeO_2$ ($N_{Cu-Cu} = 10.1$, $R = 2.55$ Å); blue: Cu/CeO_2 ($N_{Cu-Cu} = 8.9$, $R = 2.55$ Å) green: $CuPd/Al_2O_3$ ($N_{Cu-Cu} = 10.0$, $R = 2.55$ Å); pink: Cu foil ($N_{Cu-Cu} = 12$, $R = 2.55$ Å). (For interpretation of the references to color in this figure legend, the reader is referred to the web version of this article.)

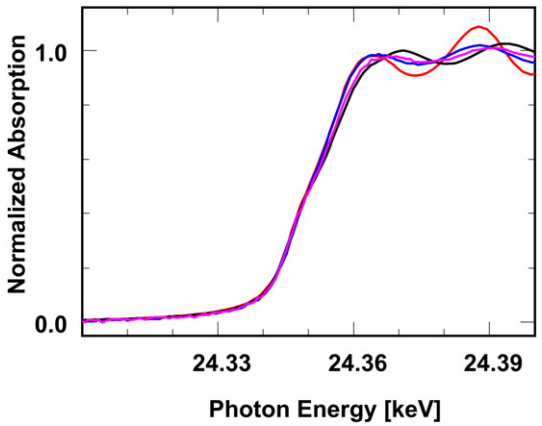

Fig. 11. Pd XANES (24.30–24.40 keV). Red: Pd foil: $N_{Pd-Pd} = 12.0$ at 2.75 Å; blue: Pd/CeO_2: $N_{Pd-Pd} = 5.7$ at 2.71 Å; black: $PdCu/Al_2O_3$: $N_{Pd-Cu} = 9.4$ at 2.57 Å; pink: $PdCu/CeO_2$: $N_{Pd-Cu} = 4.0$ at 2.55 Å. (For interpretation of the references to color in this figure legend, the reader is referred to the web version of this article.)

Table 3
Pd EXAFS fits.

Sample	Treatment	Backscatter	CN	*R*	DWF	E_0
30% Cu–1% Pd/CeO_2	4% H_2 300 °C + He at 300 °C	Pd–Cu	4.0	2.55	0.005	−2.5
1% Pd/CeO_2	4% H_2 300 °C + He at 300 °C	Pd–Pd	5.7	2.71	0.005	−2.2
30% Cu–1% Pd/Al_2O_3	4% H_2 300 °C + He at 300 °C	Pd–Cu	9.4	2.57	0.005	0.5

55 Å [26]. For the samples which contain Pd, there is no clear indication from the Cu edge that there are Pd neighbors, but the Cu content (30 wt%) is much higher than Pd (1 wt%), so further analysis was conducted at Pd edge.

3.2.1.2. Pd EXAFS and XANES The Pd *K* edge XANES of Pd foil, 1% Pd/CeO_2, 30% Cu–1% Pd/CeO_2 and 30% Cu–1% Pd/Al_2O_3 are shown in Fig. 11. The shape and position of the edge for 1% Pd/CeO_2 is similar to that of Pd foil except that the peaks have lower intensity. The XANES spectra for 30% Cu–1% Pd/CeO_2 and 30% Cu–1% Pd/Al_2O_3, however, are significantly different from that of metallic Pd indicating a different coordination environment around the Pd atoms.

The fits of the Pd EXAFS are given in Table 3. The N_{Pd-Pd} of 5.7 indicates small metallic Pd particles of approximately 15 Å [26]. Fig. 12 shows the Fourier transform of 1% Pd/CeO_2 and Pd foil. The shift to lower *R* of the imaginary part of the Fourier transform in 1% Pd/CeO_2 indicates a shorter bond distance. The Pd bond distance is 2.71 Å compared to 2.75 Å in Pd foil and is consistent with small metallic particles.

The Pd EXAFS of 30% Cu–1% Pd/CeO_2 and 30% Cu–1% Pd/Al_2O_3 are significantly different from that in metallic Pd. Fig. 13 shows the Fourier transform of 30% Cu–1% Pd/Al_2O_3 and Pd foil. The position of the metallic peak is significantly shifted to lower *R* in the catalyst. Fit of this peak with a Pd–Cu FEFF reference indicates that (metallic) Pd has about 4 Cu neighbors in 30% Cu–1% Pd/CeO_2 and 9 Cu neighbors in 30% Cu–1% Pd/Al_2O_3. The fit of the Fourier transform for the first shell Pd–Cu peak of 30% Cu–1% Pd/Al_2O_3 is given in Fig. 14. In both catalysts Pd has formed a Pd–Cu alloy where the Pd atoms are surrounded by only Cu atoms. Fig. 15 shows the Fourier transform of the two Pd–Cu catalysts. There is a small decrease in the Pd–Cu bond distance in 30% Cu–1% Pd/CeO_2, which has the smaller N_{Pd-Cu}.

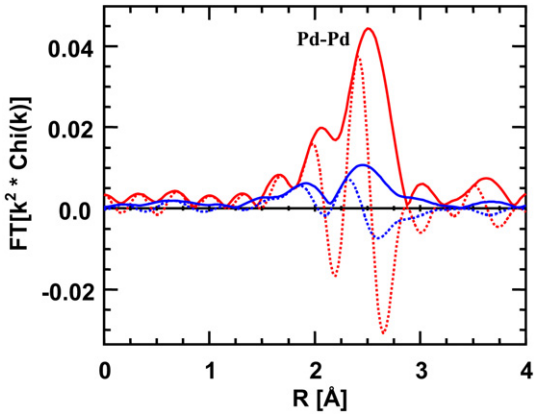

Fig. 12. Fourier transform of Pd/CeO_2 reduced at 250 °C and He at 250 °C compared with Pd foil (k^2: $\Delta k = 2.8$–12.3 Å^{-1}). Red: Pd foil: $N_{Pd-Pd} = 12.0$ at 2.75 Å; blue: Pd/CeO_2: $N_{Pd-Pd} = 5.7$ at 2.71 Å. (For interpretation of the references to color in this figure legend, the reader is referred to the web version of this article.)

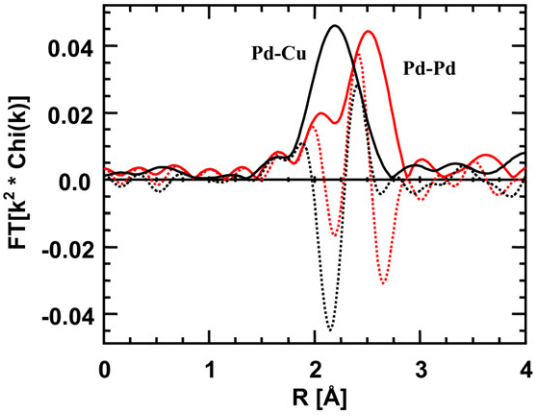

Fig. 13. Fourier transform of Pd EXAFS of $CuPd/Al_2O_3$ reduced at 250 °C and He at 250 °C compared with Pd foil (k^2: $\Delta k = 2.8$–12.3 Å^{-1}). Red: Pd foil: $N_{Pd-Pd} = 12.0$ at 2.75 Å; black: $PdCu/Al_2O_3$: $N_{Pd-Cu} = 9.4$ at 2.57 Å. (For interpretation of the references to color in this figure legend, the reader is referred to the web version of this article.)

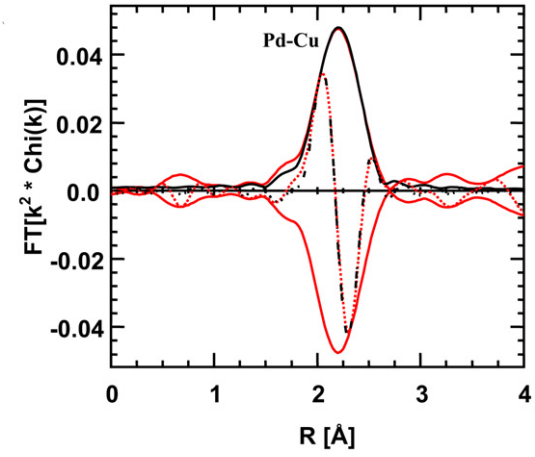

Fig. 14. Fit of the Fourier transform for $PdCu/Al_2O_3$ reduced at 250 °C and He at 250 °C (k^2: $\Delta k = 2.8$–12.3 Å^{-1}). Red solid: data, magnitude of FT; red dotted: data, imaginary part of FT; black solid: fit, magnitude FT; black dotted: fit, imaginary part of FT; fit: $N_{Pd-Cu} = 9.4$ at 2.57 Å. (For interpretation of the references to color in this figure legend, the reader is referred to the web version of this article.)

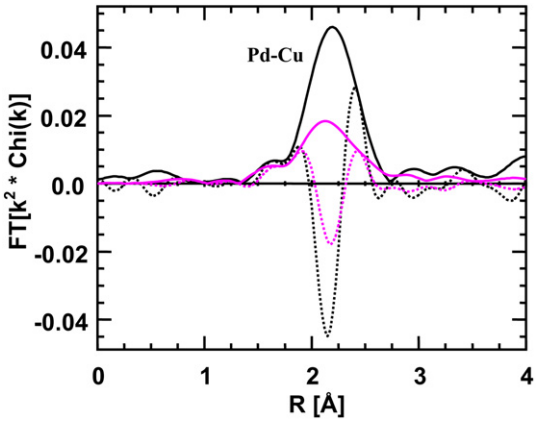

Fig. 15. Fourier transform of $PdCu/Al_2O_3$ and $PdCu/CeO_2$ reduced at 250 °C and He at 250 °C (k^2: $\Delta k = 2.8$–12.3 Å^{-1}). Black: $PdCu/Al_2O_3$: $N_{Pd-Cu} = 9.4$ at 2.57 Å; pink: $PdCu/CeO_2$: $N_{Pd-Cu} = 4.0$ at 2.55 Å. (For interpretation of the references to color in this figure legend, the reader is referred to the web version of this article.)

3.2.2. Surface properties

The surface properties of the Cu–Pd/CeO_2 catalysts have been investigated by CO chemisorption and *in situ* XPS measurements. The CO chemisorption has been used to determine the metal dispersions, and the results are included in Table 1. The monometallic Pd/CeO_2 catalyst shows a Pd dispersion of 38.5%. On the other hand, the monometallic Cu/CeO_2 catalyst shows a very low Cu metal dispersion of about 0.5%. It should be noted that CO chemisorption has not been observed in some supported Cu and Pd catalysts [27] although CO chemisorption on Cu and Pd-based catalysts are very well known [24,28–30]. In fact, in a recent study by Lambert et al. [31] on the CO chemisorption over Cu–Pd bimetallic catalysts supported on SiO_2 hypothesized that CO is chemisorbed only on Pd, but not on Cu. Consequently, the dispersion of only the Pd metal has been determined for a series of Cu–Pd/SiO_2 catalysts. Alternative approaches such as the one suggested by Vannice and co-workers [32], using N_2O adsorption, may be used to determine the dispersion of individual metal in bimetallic catalyst system. However, due to the unavailability of the experimental set up, the present authors used the CO chemisorption technique to estimate the metal dispersion of the present bimetallic catalyst system.

The dispersion data for the Cu–Pd/CeO_2 bimetallic catalyst systems shown in Table 1 gives valuable information. For instance, the metal dispersion increased from 0.5% for Cu/CeO_2 to 0.8% for CuPd/CeO_2 bimetallic catalyst. The metal dispersion further increases upon leaching with NH_3 or HNO_3. Thus, the sample leached with HNO_3 shows a metal dispersion of 29.3%. If we assume that, the CO chemisorption in the CuPd/CeO_2 bimetallic catalyst occurs only on Pd, then the observed results imply that, the presence of Cu drastically suppresses the Pd dispersion. On the other hand, if CO chemisorption on the Cu in these catalysts is significant, then the results suggest that large clusters of Cu are present on the CeO_2 surface and that the addition of Pd improves the Cu metal dispersion.

XPS studies have been performed under "pseudo *in situ*" conditions on these catalysts before and after reduction in order to further investigate the surface nature of Cu and Pd in these samples. Fig. 16 depicts the core level X-ray photoelectron (XP) spectra in the Cu 2p region for Cu/CeO_2 and CuPd/CeO_2 catalysts and their XPS parameters are summarized in Table 4. The unreduced samples exhibit XP spectra typical of Cu^{2+} with Cu $2p_{3/2}$ and $2p_{1/2}$ main peaks appearing around 933 and 952.5 eV, respectively together with strong satellite speaks on higher BE sides. However, significant differences in peak positions and full-width at half maximum (FWHM) are observed in the spectra between

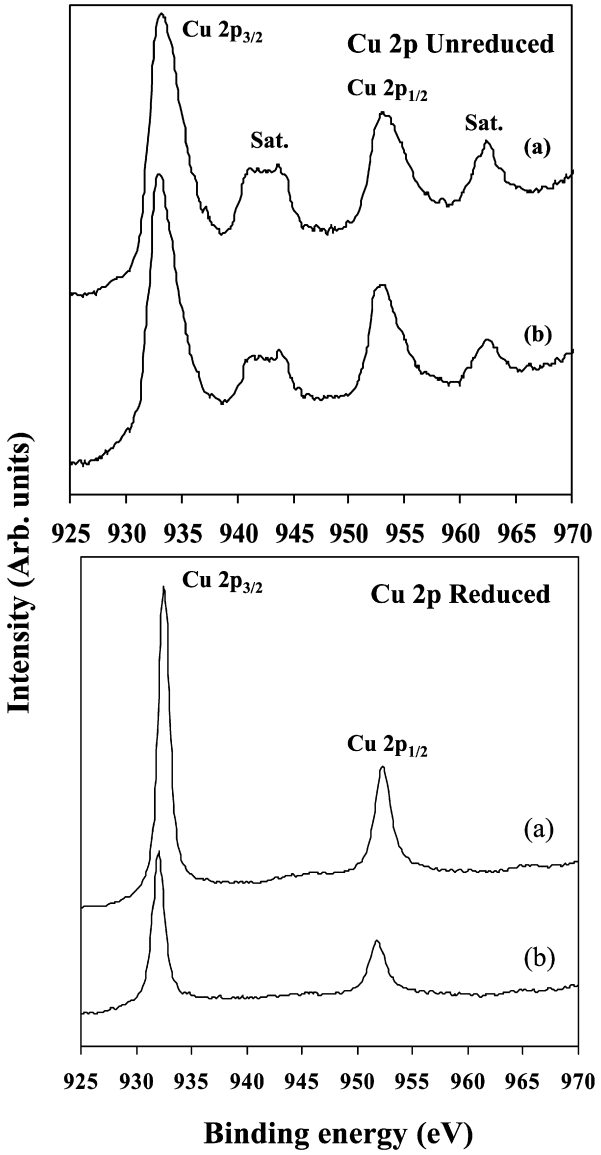

Fig. 16. Cu 2p XP spectra of (a) Cu/CeO_2; (b) CuPd/CeO_2. (Top panel) Unreduced samples; (bottom panel) reduced samples.

Table 4
Cu 2p XPS and Cu Auger parameters of CuPd/CeO_2 bimetallic catalysts.

Catalyst	BE $2p_{3/2}$ (eV)	FWHM Cu $2p_{3/2}$ (eV)	BE $2p_{1/2}$ (eV)	FWHM Cu $2p_{1/2}$ (eV)	ΔE (eV)	KE of Cu $L_3M_{45}M_{45}$ (eV)	α' (eV)
Cu/CeO_2	932.9	3.5	952.5	3.5	19.6	917.8	1850.7
CuPd/CeO_2	932.7	2.5	952.3	2.5	19.6	917.5	1850.2
Cu/CeO_2 (red.)	932.4	1.5	952.2	1.5	19.8	918.8	1851.2
CuPd/CeO_2 (red.)	932.0	1.5	951.6	1.5	19.6	919.4	1851.4
CuO[a]	934.6	–	–	–	–	917.1	1851.7
Cu_2O[a]	932.8	–	–	–	–	916.5	1849.3
Cu metal[a]	932.8	–	–	–	–	918.6	1851.4

(red.) = reduced.
[a] Ref. [40].

the monometallic and the bimetallic catalysts. The monometallic Cu/CeO_2 exhibits the Cu $2p_{3/2}$ and Cu $2p_{1/2}$ main peaks at 932.9 and 952.5 eV, respectively with a FWHM of 3.5 eV. The peak positions are shifted towards lower BE by 0.2 eV and the FWHM decreases to about 2.5 eV for the Cu–Pd/CeO_2 bimetallic catalyst. A shift in lower BE in XPS is usually associated with an increased electron density or reduction to a lower oxidation state. Thus, the

Table 5
Pd 3d XPS parameters of $CuPd/CeO_2$ bimetallic catalysts.

Catalyst	BE of $Pd_{5/2}$ (eV)	FWHM of $Pd_{5/2}$ (eV)	BE of $Pd_{3/2}$ (eV)	FWHM of $Pd_{3/2}$ (eV)	ΔE (eV)
Pd/CeO_2	337.8	1.5	343.0	1.5	5.2
$CuPd/CeO_2$	337.3	3.0	342.5	3.0	5.2
Pd/CeO_2 (red.)	335.0	1.9	340.0	1.9	5.0
$CuPd/CeO_2$ (red.)	335.3	1.6	340.3	1.6	5.0
$PdCl_2$[a]	337.8				
PdO[a]	336.3				
PdO_2[b]	337.9				
Pd metal[a]	335.0				

(red.) = reduced.
[a] Refs. [41,42].
[b] Ref. [43].

results indicate that the Cu^{2+} in the Cu/CeO_2 system becomes partially reduced when Pd is added to the Cu/CeO_2 system. This is further supported by a decrease in intensity of satellite peaks.

Upon reduction, the satellite peaks in the Cu 2p core level XP spectra disappeared and the peaks are narrowed down and shifted towards lower BE. The monometallic Cu/CeO_2 catalyst shows a sharp and intense peak at 932.4 eV for Cu $2p_{3/2}$ and at 952.2 eV for Cu $2p_{1/2}$ with a spin–orbit coupling energy of 19.8 eV. The $CuPd/CeO_2$ bimetallic catalysts shows the Cu $2p_{3/2}$ and 2p $Cu_{1/2}$ peaks at 932.0 and 951.6 eV, respectively and these are lower by 0.4–0.6 eV compared to the monometallic Cu/CeO_2 catalyst. The loss of satellite peaks and shift in the peak positions towards lower BE compared to the unreduced samples clearly indicates the reduction of Cu^{2+} to Cu^+ or metallic state (Cu^0).

A combined core level XPS and Auger electron spectroscopy (AES) should be used to distinguish the three oxidation states of Cu (Cu^0, Cu^+ and Cu^{2+}). The Cu^{2+} species can be distinguished from Cu^+ and Cu^0 from the difference in the BE (>1 eV) and also from the appearance of satellite peaks. However, because both Cu^+ and Cu^0 will have the same BE in the core level XPS (see Table 4), the KE of electron measured in the AES and the modified Auger parameter (α'), which is defined in Eq. (2), should be used to further confirm the chemical state of copper [33].

$$\alpha' = h\upsilon + (\text{KE Cu}_{\text{LMM}} - \text{KE Cu } 2p_{3/2}), \quad (2)$$

wherein, $h\upsilon$ is the energy of the incident photon, and KE Cu_{LMM} and KE Cu $2p_{3/2}$ are kinetic energy of Auger electron for the final state, $L_3M_{45}M_{45}$ and $2p_{3/2}$ core level photoelectron, respectively.

Fig. 17 shows the Auger electron (AE) spectra of unreduced (top panel) and reduced samples (bottom panel) while their KE and Auger parameters (α') are included in Table 4. The unreduced samples exhibit a main peak centering around 917.5 eV with an Auger parameter of 1850.2 eV, indicating the existence of CuO-like species. The spectra of reduced samples exhibit sharp peaks around 919 eV. The peak for the monometallic Cu/CeO_2 occurs at 918.8 eV with an Auger parameter of 1851.2 eV while for the bimetallic $CuPd/CeO_2$ system, the peak appears at relatively higher KE of 919.4 eV with an Auger parameter of 1851.4 eV. The observed KE and Auger parameters of the reduced bimetallic catalyst closely match with that of metallic copper rather than Cu^{1+} as can be seen from the data presented in Table 4. Thus, Auger electron spectra confirm that copper in the reduced catalysts are present in their metallic state.

The Pd 3d core level XP spectra of unreduced (top panel) and reduced samples (bottom panel) are shown in Fig. 18 and their XPS parameters are gathered in Table 5. The unreduced monometallic Pd/CeO_2 catalyst (top panel) exhibits an intense doublet centering at 337.8 and 343 eV, attributed to Pd $3d_{5/2}$ and Pd $3d_{3/2}$, respectively with a spin–orbit coupling energy of 5.2 eV (see Table 3). The doublet for $CuPd/CeO_2$ bimetallic catalyst appears at

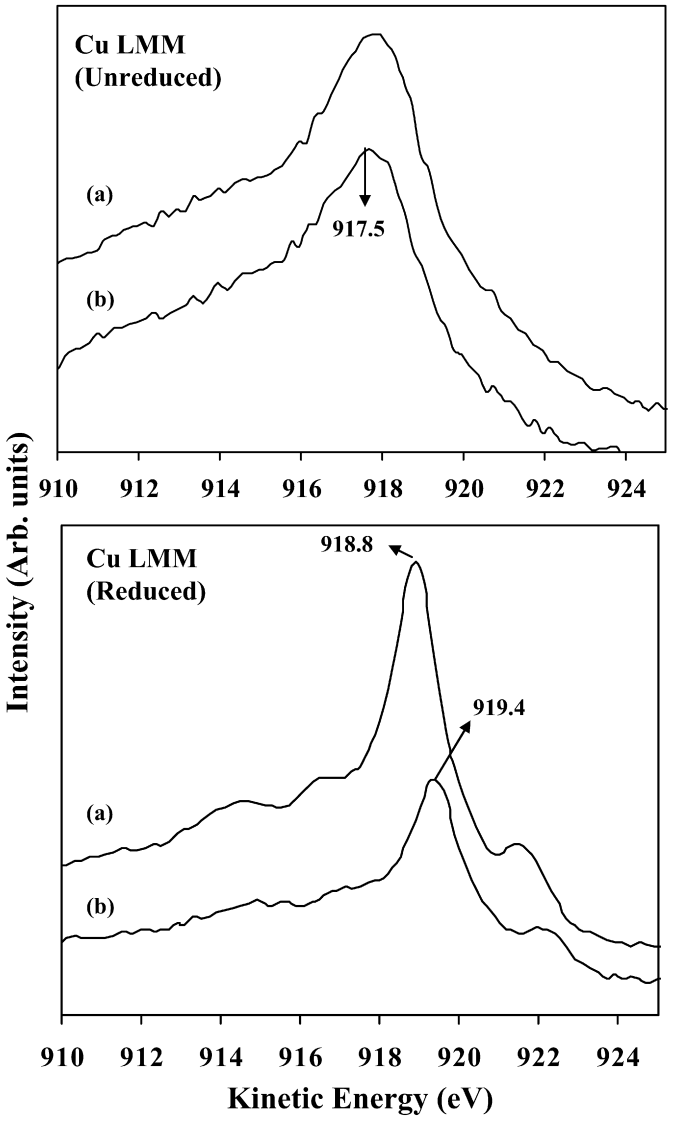

Fig. 17. Cu LMM Auger electron spectra of (a) Cu/CeO_2; (b) $CuPd/CeO_2$. (Top panel) Unreduced samples; (bottom panel) reduced samples.

relatively lower BE of 337.3 and 342.5 eV, respectively. The observed BE values closely match with that of $PdCl_2$ and PdO_2 but slightly higher compared to that reported for PdO (336.3 eV) as shown in Table 5. Since the Pd precursor used in the present study was $Pd(CH_3COO)_2$ but not $PdCl_2$, the observed BE should be better interpreted for PdO having a lower electron density on Pd^{2+} cation or species similar to that of PdO_2. The shift in the BE by 0.5 eV toward lower BE and broadening of the peaks (FWHM = 3 eV) in the bimetallic $CuPd/CeO_2$ catalyst compared to the monometallic Pd/CeO_2 (FWHM = 1.5 eV) indicates that the PdO species are highly dispersed in the Cu/CeO_2 matrix and as a consequence they are more cationic than does in the monometallic catalyst.

The reduced samples also exhibit similar doublets, but relatively at lower BE (Fig. 18, bottom panel). The Pd $3d_{5/2}$ and $3d_{3/2}$ peaks in monometallic Pd/CeO_2 occurs at 335 and 340 eV together with a shoulder at 337 eV, indicating the existence of Pd metal along with a fraction of PdO species. This peak is vanished in the $CuPd/CeO_2$ bimetallic catalyst system, indicating that Cu aids the reduction of Pd cations. Furthermore, the peaks are shifted by 0.3 eV towards higher BE, suggesting the existence of more cationic Pd species. Note that the Cu 2p peak is shifted towards lower BE and the intensity is decreased dramatically upon addition of Pd (see Fig. 16,

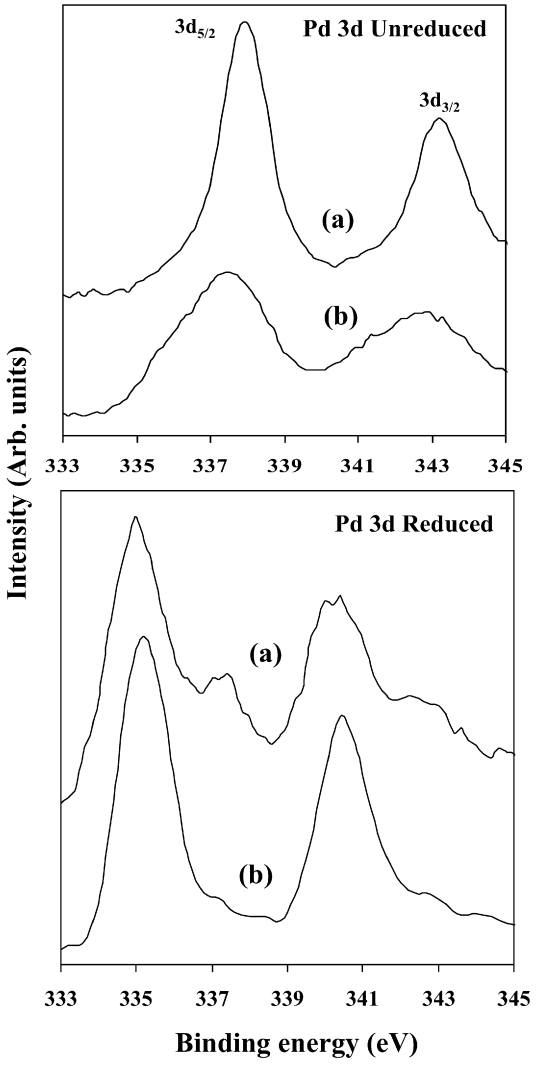

Fig. 18. Pd 3d XP spectra of (a) Pd/CeO_2; (b) $CuPd/CeO_2$. (Top panel) Unreduced samples; (bottom panel) reduced samples.

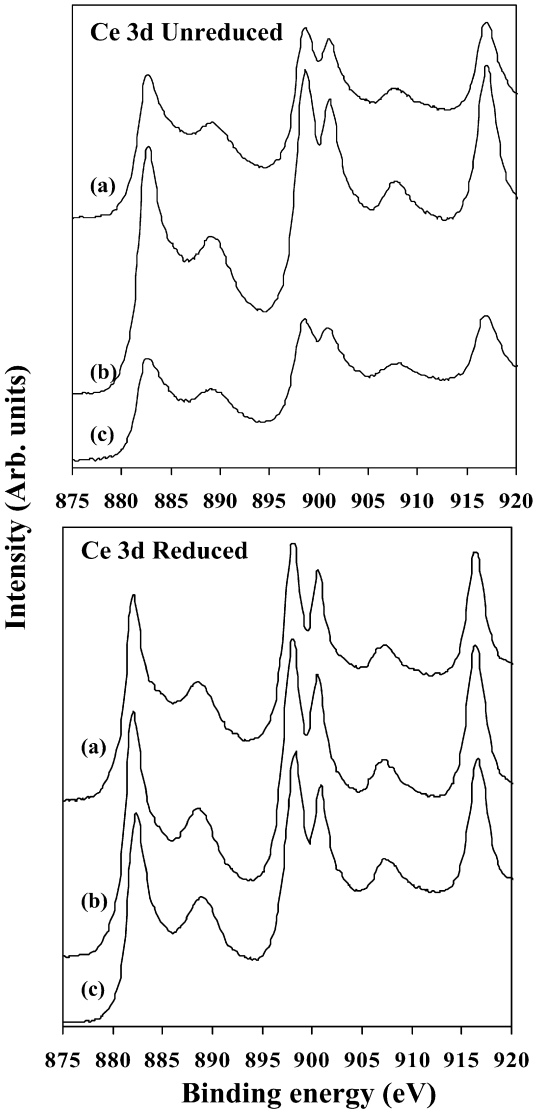

Fig. 19. Ce 3d XP spectra of (a) Cu/CeO_2; (b) Pd/CeO_2, (c) $CuPd/CeO_2$. (Top panel) Unreduced samples; (bottom panel) reduced samples.

Table 6
Surface chemical compositions of $CuPd/CeO_2$ catalysts determined by XPS.

Catalyst	Unreduced (at%)				Reduced (at%)			
	O	Cu	Pd	Ce	O	Cu	Pd	Ce
Pd/CeO_2	69.5	–	1.8(3.6)	28.7	68.2	–	1.2(2.3)	30.6
Cu/CeO_2	58.6	24.5(32.3)	–	16.6	50.7	25.1(27.5)	–	24.2
$CuPd/CeO_2$	60.0	19.0(23.9)	1.8(3.8)	19.2	56.2	16.0(17.6)	1.2(2.2)	26.6

Values in parentheses are wt%.

bottom panel). The observed results indicate the existence of a strong interaction between these two metals. It suggests that there is a modification of the electron density on the metal sites, such as a shift in electron transfer from Pd to Cu.

The surface chemical compositions determined from XPS peaks are summarized in Table 6. The results indicate that the surface concentration of Pd decreased from 1.8 to 1.2 at% in both Cu-free and Cu-containing Pd/CeO_2 catalysts upon reduction. While the Cu concentration remains almost unchanged in the Pd-free Cu/CeO_2 sample, it decreased from 19.0 at% (23.9 wt%) to 16.0 at% (17.6 wt%) upon reduction. In contrast to Pd and Cu concentrations, the Ce concentration in all the sample increased upon reduction. It can be inferred from these results that a part of Pd diffuse inward into the CeO_2 support upon reduction. However, the inward diffusion of a part of Cu occurs in the presence of Pd. These inward diffusions of Pd and Cu in these catalysts make the Ce concentrations at the surface to increase upon reduction. A similar inward diffusion of copper upon reduction treatment of $CuPd/SiO_2$ catalyst is known in the literature [34].

Fig. 19 exhibits the XP spectra of unreduced and reduced catalysts of the present study in the Ce 3d region. At least six peaks centering around 882, 889, 899, 901, 908 and 917 eV are observed in both unreduced and reduced samples and they are assigned to Ce $3d_{5/2}$ $4f^2$, Ce $3d_{5/2}$ $4f^1$, Ce $3d_{5/2}$ $4f^0$, Ce $3d_{3/2}$ $4f^2$, Ce $3d_{3/2}$ $4f^1$ and Ce $3d_{3/2}$ $4f^0$, respectively for Ce^{4+} species in CeO_2 [35,36]. Peaks for Ce^{3+} are not observed even in the reduced samples. This is in contrast to our recent results on similar Ni–Rh bimetallic catalysts supported on CeO_2, wherein a part of Ce was found in 3+ oxidation state [37]. The retention of Ce in 4+ oxidation state even after reduction in the present catalysts could be due to the lower reduction temperature of around 225 °C employed compared to 433 °C employed in a $NiRh/CeO_2$ bimetallic system. The major difference between XP spectra of unreduced and reduced samples in the Ce 3d region is that the reduction treatment improved the

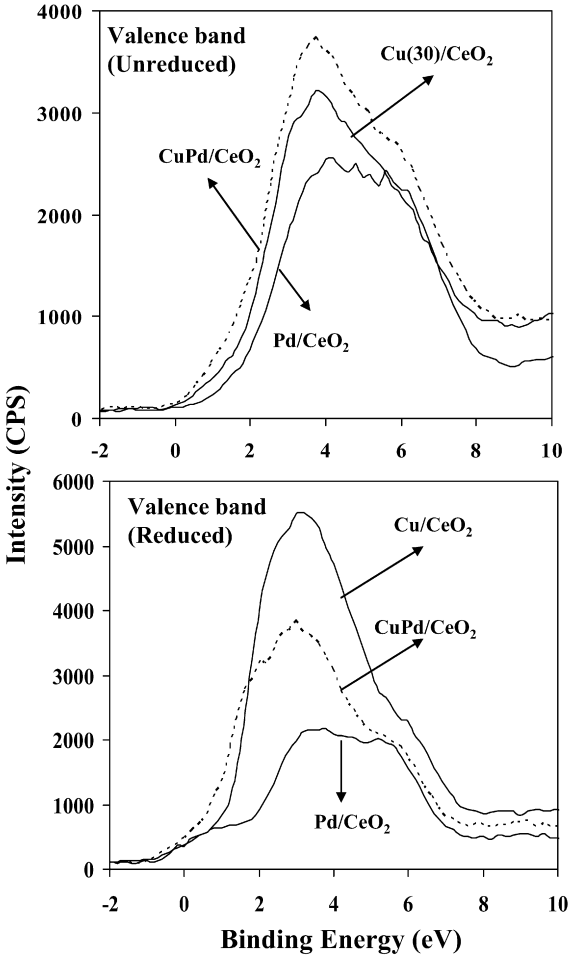

Fig. 20. Valence band XP spectra of CeO_2 supported CuPd-bimetallic catalysts. (Top panel) Unreduced samples; (bottom panel) reduced samples.

peak intensity and this is due to an increase in the surface Ce contraction as a consequence of inward diffusion of a part of Pd and Cu metals upon reduction as discussed above.

XP spectra in the valance band region, below 15 eV were also collected in order to understand the electronic structure of the materials as these bands are essentially involved in delocalization or chemical bonding. The spectra in the present study recorded below 10 eV for both unreduced and reduced samples are depicted in Fig. 20. The unreduced Pd/CeO_2 shows band maximum around 4 eV due to the contributions from various final states of Pd 4d orbital. The band structure becomes relatively sharp, intense and shifted towards lower BE, around 3.7 eV, when Cu is present in the sample and this is attributed to contributions from Cu 3d orbitals of Cu^{2+} species [38].

The valence band spectra of reduced samples (bottom panel) show that the overall spectral intensity decreases upon addition of Pd and the peaks, especially for Cu-containing samples, further shifted towards lower BE of around 3 eV. This peak corresponds to 3d orbital of metallic copper [38]. The observed results further support the core level XPS observations that the surface Cu concentration decreases upon Pd addition, especially upon reduction. Also, significant signal intensity could be seen near the Fermi level ($E_F = 0$) in the Cu-containing samples, suggesting that Cu 3d bands are located close to the Fermi energy and that the Cu species in the present $CuPd/CeO_2$ bimetallic catalysts are more effectively involved in the catalytic reaction.

4. Discussion

4.1. Nature of Cu and Pd surface species

One of the prime objectives of the present research was to elucidate the chemical nature and distribution of Cu and Pd on the catalyst surface and correlate with observed catalytic properties. Depending upon the nature of metals and support used, the metals in the bimetallic catalyst systems are known to have a strong synergistic interaction and/or highly dispersed metal particles with surface segregation of either of the metal [34,39]. The disappearance of high temperature CuO reduction peak and broadening of PdO reduction peak around 160 °C in TPR of the present $CuPd/CeO_2$ bimetallic catalyst system (Fig. 5) suggest that both CuO and PdO are reduced together and they are in close interaction with each other. This is supported by the EXAFS analysis at the Cu and Pd K edges, which showed that Pd is surrounded only by Cu atoms. A dramatic drop in Pd dispersion from 38.5% for the monometallic Pd/CeO_2 to below 1% for the bimetallic $CuPd/CeO_2$ (see Table 1) clearly indicates that the CO chemisorption is impaired upon Cu addition, supporting the above conclusion. The decrease in Cu 2p BE by 0.4 to 0.6 eV and concomitant increase in the BE of Pd in Pd 3d XP spectra of reduced $CuPd/CeO_2$ bimetallic catalysts compared to their respective monometallic Cu/CeO_2 and Pd/CeO_2 systems substantiates the TPR and CO chemisorption results and this further substantiates the conclusion on the existence of a synergistic interaction between these two metals.

The Cu 2p XPS of reduced samples indicate a dramatic decrease in intensity (Fig. 16, bottom panel) and surface Cu content upon Pd addition. However, the surface Pd content remains largely unaffected by the presence of Cu (see Table 6). These results suggest that most of the added Pd stays on the surface while significant amount of Cu is diffused or distributed in deeper layers, below the surface. This is highly possible, taking into account a large amount (25–30 wt%) of Cu loading (see Table 1) and also because, the $CuPd/CeO_2$ bimetallic catalyst in the present study has been prepared by co-impregnation by depositing Cu and Pd on the CeO_2 [13]. The observed results are in agreement with Batista et al. [40] who, by means of AES depth profile analysis on $Cu–Pd/Al_2O_3$ catalyst, have reported the distribution of Cu in deeper layers below the surface of alumina support and Pd being on the top of the Cu layer for catalyst synthesized by a similar impregnation method.

4.2. The role of Cu and Pd

The catalytic data on OWGS reaction shown in Fig. 2 indicates that an improved catalytic activity and stability could be achieved when both Pd and Cu are present together. The monometallic Cu/CeO_2 is more active but undergoes rapid deactivation, probably due to metal sintering and reoxidation of Cu metal under the present operating conditions. Deactivation has also been observed over the monometallic Pd/CeO_2 catalyst in WGS reaction and the observed result has been attributed to metal sintering [19]. It is likely that the close interaction between Cu and Pd metals of the present bimetallic catalyst system prevents both Cu and Pd from sintering, thereby improving the catalyst stability. In addition, differential scanning calorimetry experiments showed exotherms at much higher temperature than the monometallic Cu/CeO_2 and this indicated that the $CuPd/CeO_2$ bimetallic catalyst was significantly less pyrophoric than the Cu/CeO_2 catalyst (unpublished results). Thus, it can be concluded that, the addition of the second metal, Pd or Cu to the monometallic Cu/CeO_2 or Pd/CeO_2 improves the catalytic performance for CO conversion and catalyst stability and this is due to the existence of a synergistic effect between these two metals. Based on the valence band XP spectra (Fig. 10), it is

likely that Cu is more involved in the catalytic reaction and that added Pd improves the performance and stability of the catalyst.

The results from EXAFS analysis indicate the formation of Pd–Cu alloys in the presence of free Cu. Alloy formation at the Pd edge is in line with the TPR spectra that shows decreases in TPR peak temperatures of CuO upon Pd addition and there are two distinct regions of reduction for $CuPd/CeO_2$. The first region at lower temperature may be attributed to the Pd–Cu sites, while the higher temperature reduction peak may be more due to CuO particles. It is likely that Pd addition helps to keep Cu in reduced state under OWGS conditions and thus improves the catalyst stability. The higher coordination number of Pd–Cu on Al_2O_3 (9 Cu atoms surrounding each Pd atom) versus CeO_2 (4 Cu atoms surrounding each Pd atom) could also partly account for the increased activity of the ceria supported Cu–Pd catalyst. These results in combination with recent studies [44,45] are important for developing a fundamental understanding of $Cu–Pd/CeO_2$ catalyst and for further improved catalytic performance for hydrogen production.

5. Conclusions

The present study leads to the following important conclusions:

(1) The $CuPd/CeO_2$ bimetallic catalysts containing 20–30 wt% Cu and 0.5–1 wt% Pd are more active compared to the monometallic Pd/CeO_2 and Cu/CeO_2 catalysts in the oxygen-assisted water–gas shift (OWGS) reaction performed under H_2-rich conditions, especially at lower reaction temperature, below 200 °C. The bimetallic catalyst exhibits a stable CO conversion activity during 3 days of on-stream operation. The higher activity and stability of the bimetallic catalyst has been attributed to the existence of a synergistic interaction between Cu and Pd in the CeO_2-supported bimetallic catalysts.

(2) Addition of Pd to Cu/CeO_2 system decreased the surface Cu concentration, especially upon reduction, while the surface concentration of Pd remains unaffected by the presence of Cu in these catalysts. The lower coordination number of Pd in Pd–Cu on CeO_2 (4 Cu atoms surrounding each Pd atom), compared to that on Al_2O_3 (9 Cu atoms surrounding each Pd atom) as revealed by EXAFS, could also partly account for the increased activity of the CeO_2-supported Cu–Pd catalyst.

(3) A significant charge transfer between Cu and Pd occur with Cu being more electron rich and Pd being electron deficient. Such synergistic interaction exists even in their oxidic state of the present catalyst system.

(4) In the $CuPd/CeO_2$ bimetallic catalyst system, Cu metal could be more effectively involved in the catalytic reaction for the conversion of CO by OWGS. The addition of Pd further improves the performance and stability of copper catalyst.

(5) Cu loading has an impact on the catalytic performance of $CuPd/CeO_2$ bimetallic catalysts in the OWGS reaction. Catalyst containing 20–30 wt% Cu was found to be more active compared to that containing lower Cu loading of about 1 wt% obtained by HNO_3 leaching.

(6) EXAFS analysis indicates the Pd–Cu alloy is formed at the Pd edge, which explains the increase in stability and durability of the catalysts over the monometallic counterparts. EXAFS, TPR, XPS and catalytic reaction data in combination suggest that Pd addition helps to keep Cu in reduced state and thus improves the catalyst stability.

Acknowledgments

Partial funding from US Department of Energy, National Energy Technology Laboratory and ConocoPhillips Petroleum Corp. for our earlier project on methanol reforming, including water–gas shift for hydrogen production, which led to the reactor system set-up at Penn State for the current work, and technical assistance from the Penn State Materials Characterization Lab for ICP-AES are gratefully acknowledged. A portion of the research described in this paper was performed in the Environmental Molecular Sciences Laboratory, a national scientific user facility sponsored by the Department of Energy's Office of Biological and Environmental Research and located at Pacific Northwest National Laboratory. Use of the Advanced Photon Source was supported by the US Department of Energy, Office of Basic Energy Sciences, Office of Science (DOE-BES-SC), under Contract No. W-31-109-Eng-38. The MR CAT is funded by the member institutions and DOE-BES-SC under Contracts DE-FG02-94ER45525 and DE-FG02-96ER45589. We also acknowledge partial funding of this work from NSF GOALI 99-04033 grant.

References

[1] C.S. Song, Catal. Today 77 (2002) 17–49.
[2] L.F. Brown, Int. J. Hydrogen Energy 26 (2001) 381–397.
[3] J.R. Rostrup-Nielson, T. Rostrup-Nielson, Cattech 6 (2002) 150–159.
[4] S. Velu, K. Suzuki, Top. Catal. 22 (2003) 235–244.
[5] A. Ghenciu, Solid State Mater. Sci. 1 (2002) 389–399.
[6] G.A. Deluga, J.R. Salge, L.D. Schmidt, X.E. Verykios, Science 303 (2004) 993–997.
[7] D.L. Trimm, Z.I. Onsan, Catal. Rev. Sci. Eng. 43 (2001) 31–84.
[8] J.D. Holladay, Y. Wang, E. Jones, Chem. Rev. 104 (2004) 4767–4790.
[9] J.M. Zalc, D.G. Loffler, J. Power Sources 111 (2002) 58–64.
[10] N.A. Koryabkina, A.A. Phatak, W.F. Ruettinger, R.J. Farrauto, F.H. Ribeiro, J. Catal. 217 (2003) 233–239.
[11] T. Utaka, K. Sekizawa, K. Eguchi, Appl. Catal. A 194–195 (2000) 21–26.
[12] Q. Fu, H. Saltsburg, M. Flytzani-Stephanopoulos, Science 301 (2003) 935–938.
[13] E.S. Bickford, S. Velu, C.S. Song, Catal. Today 99 (2005) 347–357.
[14] G.C. Chinchen, M.S. Spencer, K.C. Waugh, D.A. Whan, J. Chem. Soc. Faraday Trans. 83 (1987) 2193–2212.
[15] L. Jiang, G.-C. Wang, Z.-S. Cai, Y.-M. Pan, X.-Z. Zhao, J. Mol. Struct. (Theochem) 710 (2004) 97–104.
[16] J. Kugai, S. Velu, C.S. Song, Catal. Lett. 101 (2005) 255–264.
[17] S. Velu, C.S. Song, M.H. Engelhard, Y.-H. Chin, Ind. Eng. Chem. Res. 44 (2005) 5740–5749.
[18] T. Bunluesin, R.J. Gorte, G.W. Graham, Appl. Catal. B 15 (1998) 107–114.
[19] X. Wang, R.J. Gorte, J.P. Wagner, J. Catal. 212 (2002) 225–230.
[20] G. Glaspell, L. Fuoco, M.S. El-Shall, J. Phys. Chem. B 109 (2005) 17350–17355.
[21] K. Li, Q. Fu, M. Flytzani-Slephanopoulos, Appl. Catal. B 27 (2000) 179–191.
[22] X. Qi, M. Flytzani-Slephanopoulos, Ind. Eng. Chem. Res. 43 (2004) 3055–3062.
[23] H. Zhu, Z. Qin, W. Shan, W. Shen, J. Wang, J. Catal. 223 (2005) 41–50.
[24] X. Tang, B. Zhang, Y. Li, Y. Xu, Q. Xin, W. Shen, Appl. Catal. A 288 (2005) 116–125.
[25] W. Liu, M. Flytzani-Stephanopoulos, J. Catal. 153 (1995) 317–332.
[26] J.T. Miller, A.J. Kropf, Y. Zha, J.R. Regalbuto, L.L. Delannoy, E. Bus, J.R. van Bokhoven, J. Catal. 240 (2006) 222–234.
[27] L.S. Vadlamannati, V.I. Kovalchuk, J.L. d'Itri, Catal. Lett. 58 (1999) 173–178.
[28] J.J.F. Scholten, A.P. Pijpers, A.M.L. Hustings, Catal. Rev. Sci. Eng. 27 (1985) 151–206.
[29] P. Canizares, A. de Lucas, F. Dorado, A. Duran, I. Asencio, Appl. Catal. A 169 (1998) 137–150.
[30] J. Panpranot, K. Pattamakomsan, P. Prasserthdam, J.G. Goodwin, Ind. Eng. Chem. Res. 43 (2004) 6014–6020.
[31] S. Lambert, B. Heinrichs, A. Brasseur, A. Rulmont, J.-P. Pirard, Appl. Catal. A 270 (2004) 201–208.
[32] M.H. Kim, J.R. Ebner, R.M. Friedman, M.A. Vannice, J. Catal. 208 (2002) 381–392.
[33] S. Velu, K. Suzuki, C.S. Gopinath, J. Phys. Chem. B 106 (2002) 12737–12746.
[34] A.M. Venezia, L.F. Liotta, G. Deganello, Z. Schay, L. Guczi, J. Catal. 182 (1999) 449–455.
[35] M.A. Henderson, C.L. Perkinds, M.H. Engelhard, S. Theyuthasan, C.H.F. Peden, Surf. Sci. 526 (2003) 1–18.
[36] J.P. Holgado, G. Munuera, J.P. Espinos, A.R. Gonzalez-Elipe, Appl. Surf. Sci. 158 (2000) 164–171.
[37] J. Kugai, S. Velu, C.S. Song, M.H. Engelhard, Y.-H. Chin, J. Catal. 238 (2006) 430–440.
[38] S. Velu, K. Suzuki, M. Vijayaraj, S. Barman, C.S. Gopinath, Appl. Catal. B 55 (2005) 287–299.
[39] M. Chen, D. Kumar, C.-W. Yi, D.W. Goodman, Science 310 (2005) 291–293.
[40] J. Batista, A. Pintar, D. Mandrino, M. Jenko, V. Martin, Appl. Catal. A 206 (2001) 113–124.

[41] W.-J. Shen, Y. Matsumura, Phys. Chem. Chem. Phys. 2 (2000) 1519–1522.
[42] R. Gopinath, N. Lingaiah, B. Sreedhar, I. Suryanarayana, P.S.S. Prasad, A. Obuchi, Appl. Catal. B 46 (2003) 587–594.
[43] D. Briggs, M.P. Seah (Eds.), Practical Surface Analysis: Auger and X-Ray Photoelectron Spectroscopy, Wiley, 1990.
[44] C.S. Song, Top. Catal. 49 (1–2) (2008) 1–3.
[45] E.B. Fox, A.F. Lee, K. Wilson, C.S. Song, Top. Catal. 49 (2008) 89–96.